Supplemental information

Inventory of Supplemental Information

1. Figure S1 is related to Figure 2.
2. Figure S2 is related to all main text Figures.
3. Figure S3 is related to all main text Figures.
4. Figure S4 is related to Figures 3 and 4.
5. Figure S5 is related to Figure 4.
6. Figure S6 is related to Figure 5.
7. Figure S7 is related to Figure 6.
8. Table S1 is related to Material and Methods section.

Supplementary Figures and legends

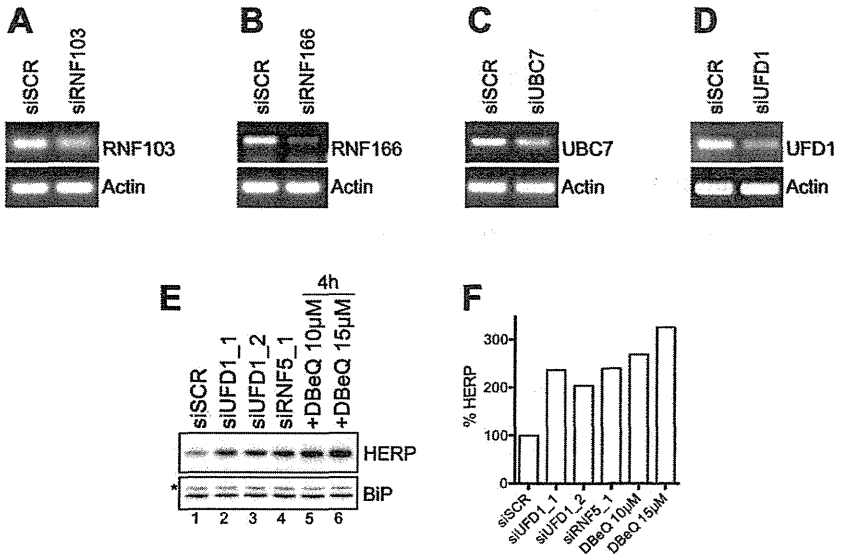

Figure S1, related to Figure 2. Controls of gene silencing and of UFD1/p97 involvement in the constitutive disposal of HERP. Silencing of RNF103 (**A**), RNF166 (**B**), UBC7 (**C**) and UFD1 (**D**) were monitored by RT-PCR. **E**, HERP and BiP levels (Western blots) in mock (siSCR) or upon silencing of select genes or in cells incubated with 10/15µM DBeQ for 4 h. The asterisk shows a cross-reacting protein. **F**, Variations in the level of HERP was quantified and plotted.

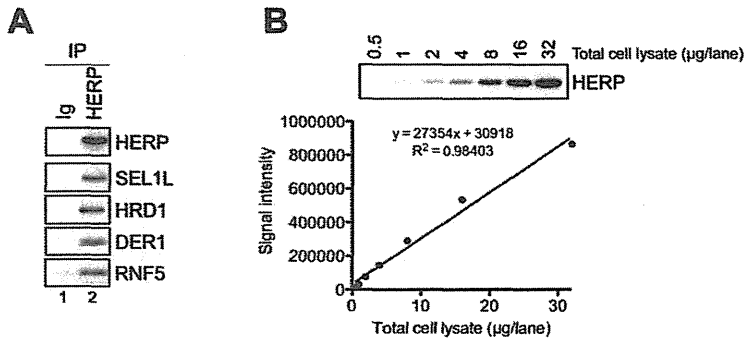

Figure S2, related to all main text Figures. Controls of immunoprecipitation and Western blot linearity. A, Lysates were immunoprecipitated with control antiserum (lane 1) or with anti-HERP antiserum (lane 2) and the associated SEL1L, HRD1, DER1 and RNF5 were detected by Western blot. **B**, Linearity of the Western blot signal was determined by calculating the coefficient of determination (R^2).

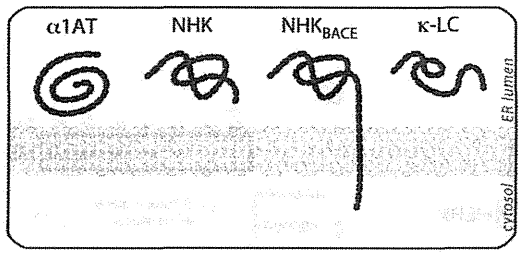

Model protein	Secretory	ERAD-L$_S$	ERAD-L$_M$	ERAD-L$_S$
HRD1/HERP substrate	No	Yes	No	Yes
HERP stabilization	No	Yes	No	Yes

Figure S3, related to all main text Figures. Schematic representation of the four model proteins used in this study. α1AT is a soluble folding-competent secretory protein. NHK and NHK$_{BACE}$ are the soluble and membrane-anchored folding-defective ERAD-L$_S$ and ERAD-L$_M$ variants of α1AT, respectively. κ-LC is an ERAD-L$_S$ substrate.

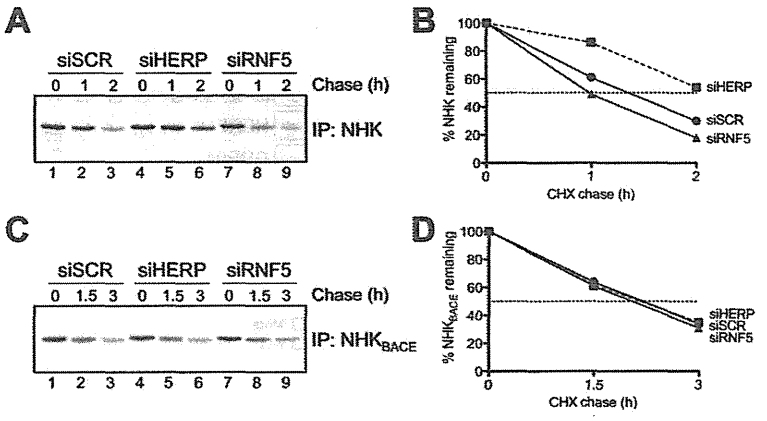

Figure S4, related to Figures 3 and 4. Consequences of HERP or RNF5 silencing on NHK and NHK_{BACE} clearance. **A**, Radiolabeled NHK was immunoisolated after the indicated chase times from mock-treated cells (siSCR, lanes 1-3), and from cells with reduced levels of HERP (lanes 4-6) or RNF5 (lanes 7-9). **B**, Quantification of **A**. **C**, Same as **A** for NHK_{BACE}. **D**, Same as **B**.

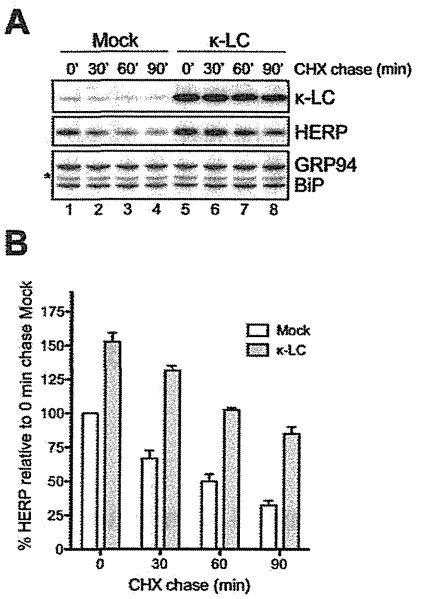

Figure S5, related to Figure 4. κ-LC expression delays HERP turnover. A, HERP turnover (second panel) has been analyzed by CHX chase in cells not-induced (lanes 1-4, $t_{1/2}$ of 60 min) or induced for expression of the misfolded protein κ-LC (lanes 5-8, $t_{1/2}$ of 90 min, induction with 100 ng/ml tetracycline for 5 h) and quantified (**B**). The κ-LC-induced delay in HERP turnover leads to a 1.5 folds increased steady state level of HERP in cells expressing κ-LC compared to cells not expressing the transgene (second panel, lanes 5 *vs* 1). The asterisk shows a cross-reacting protein. Error bars: standard deviations from the mean of 2 replicates.

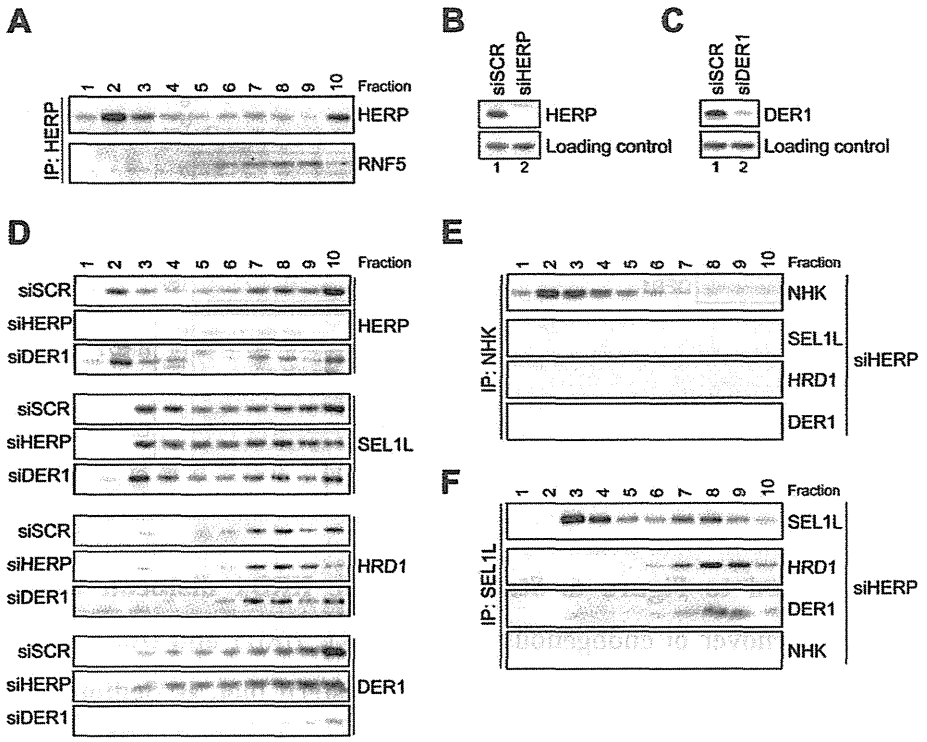

Figure S6, related to Figure 5. Sedimentation of RNF5:HERP complexes and integrity of the HRD1 dislocon in sucrose gradients. **A**, HERP from mock-treated cells was immunoisolated from each sucrose gradient fraction (first panel). The associated RNF5 was detected by Western blot (second panel). HERP:RNF5 complexes are quite large (they sediment in fractions 5-9 corresponding to 400-700 kDa). It is possible that UBC6e (shown in Fig. 2 to be involved, with RNF5, in the regulation of the constitutive turnover of endogenous HERP) as well as other factors do participate in these complexes. **B**, Level of HERP in mock-treated cells (siSCR, lane 1) and in cells with reduced HERP expression (siHERP, lane 2). Actin is shown as a loading control. **C**, Same as **B** for DER1. **D**, Sedimentation of endogenous HERP, SEL1L, HRD1 and DER1 in mock-treated cells (siSCR) or in cells silenced for HERP or DER1 expression (siHERP, siDER1). **E**, NHK (induced for 16 h with 10 ng/ml tetracycline) in cells with reduced HERP levels was immunoisolated from each fraction (first panel) and the associated SEL1L, HRD1 and DER1 were detected by Western blot. **F**, Same as **E** where SEL1L was immunoisolated.

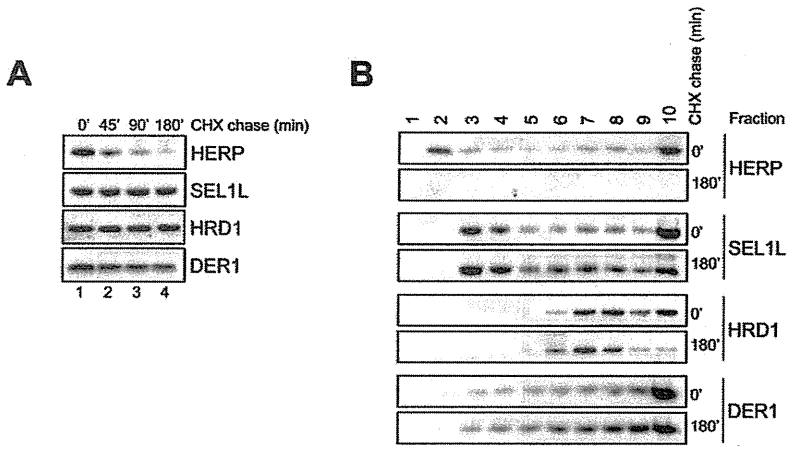

Figure S7, related to Figure 6. Stability of the HRD1 dislocon in sucrose gradients. **A**, Turnover of endogenous HERP, SEL1L, HRD1 and DER1 in HEK293 cells was analyzed by CHX chase followed by Western blot. **B**, Sedimentation of endogenous HERP, SEL1L, HRD1 and DER1 in mock cells (0 min CHX chase) or in cells incubated for 180 min with CHX (180 min CHX chase).

Supplementary table and legend

A

Protein	Oligo name	siRNA sequence
gp78	gp78	GACGGAUUCAAGUACCUUUTT
HERP	HERP	GUGCUUUACUUUAAACUAATT
HRD1	HRD1	GGUGAUGGGCAAGGUGUUCTT
RNF5	RNF5_1 RNF5_2 RNF5_3	GGGCGCGACCTTCGAATGTAA AACGGCAAGAGTGTCCAGTAT CACCGTCTTCAATGCCCATGA
RNF103	RNF103	CCCGAGGTAAATGATCTGTTT
RNF166	RNF166	CAGTTACTCTTCATATTGCAA
UBC6e	UBC6e_1 UBC6e_2	CAGCATCCTTTCATCAACCTA TAGCAGTTACGTCCTGCTTAA
UBC7	UBC7	CAGGTTGATTCCTTATGCAAA
UFD1	UFD1_1 UFD1_2	GTGGAGAGCGTCAACCTTCAA GACTAAATTGTCTAACATGAA

B

Gene	Primer sequence forward	Primer sequence reverse
β-actin	CTTCCTGGGCATGGAGTCCT	GGAGCAATGATCTTGATCTT
BiP	GAGTTCTTCAATGGCAAGGA	CCAGTCAGATCAAATGTACCC
GRP94	CTGGGACTGGGAACTTATGAATG	TCCATATTCGTCAAACAGACCAC
HERP	CCGGTTACACACCCTATGGG	TGAGGAGCAGCATTCTGATTG
RNF103	CATTGTGGTGGTATGAAACTGGCA	CCCGGCACTCCAAAATGGT
RNF166	TCACAGCCTATCCCCAGCAA	AGGAGAACTTGTGTCGGTGAA
UBC7	AGGTGGTGTTTTTAAGGCTCATC	CATTTGGGTGCCAGATTTCTGTA
UFD1	GCCACCTACTCCAAATTCCA	CAATGATGGACACTGCCTTG
u+sXbp1	TGCGGAGGAAACTGAAAAAC	TGGCTGGATGAAAGCAGATT

Table S1, related to Material and Methods section. siRNA and primers sequences. siRNA (**A**) and RT-PCR primers sequences (**B**) used in this study. u+sXbp1: primer for amplification of both unspliced and spliced Xbp1.

EN-13–1425/NDRG1 deficiency attenuates fetal growth and the intrauterine response to hypoxic injury

[1]Jacob Larkin, [2]Baosheng Chen, [1]Xiao-Hua Shi, [1]Takuya Mishima, [3]Koichi Kokame, [1,4]Yaacov Barak, [1,4]Yoel Sadovsky

1Magee-Womens Research Institute, Department of Obstetrics, Gynecology and Reproductive Sciences, University of Pittsburgh, Pittsburgh, PA, [2]Department of Obstetrics and Gynecology, WA University, St Louis, MO, [3]Department of Molecular Pathogenesis, National Cerebral and Cardiovascular Center, Osaka, Japan, [4]Department of Microbiology and Molecular Genetics, University of Pittsburgh, Pittsburgh, PA.

Intrauterine mammalian development depends on the preservation of placental function. The expression of the protein N-myc downstream–regulated gene 1 (NDRG1) is increased in placentas of human pregnancies affected by fetal growth restriction and in hypoxic primary human trophoblasts, where NDRG1 attenuates cell injury. We sought to assess the function of placental NDRG1 *in vivo*, and tested the hypothesis that NDRG1 deficiency in the mouse embryo impairs placental function and consequently, intrauterine growth. We found that *Ndrg1* knock-out (KO) embryos were growth restricted in comparison to wild-type or heterozygous counterparts. Furthermore, hypoxia reduced the survival of female, but not male, KO embryos. *Ndrg1* deletion caused significant alterations in placental gene expression, with a marked reduction in transcription of several lipoproteins in the placental labyrinth. These transcriptional changes were associated with reduced fetal:maternal serum cholesterol ratio exclusively in female embryos. Collectively, our findings indicate that NDRG1 promotes fetal growth, and regulates the metabolic response to intrauterine hypoxic injury in a sexually dichotomous manner.

Eutherian fetal development and growth depend on the placenta, which regulates maternal-fetal exchange and executes essential transport, metabolic, immune and endocrine functions. Placental injury stemming from hypoxia, oxidative stress or inflammatory insults can impede normal intrauterine development, leading to fetal death or fetal growth restriction (FGR) and the resulting perinatal and neonatal morbidity and mortality, medically induced prematurity, and adult metabolic disease (1–4). Despite the significant burden of disease associated with placental dysfunction, mechanisms underlying placental function and the adaptive response to injury remain poorly understood.

N-Myc Downstream Regulated Gene 1 (NDRG1) is a 43 kDa, evolutionarily conserved stress-response protein (5, 6). A homozygous nonsense mutation of *NDRG1* results in the demyelinating peripheral neuropathy Charcot-Marie-Tooth 4D (CMT4D), with a similar phenotype in *Ndrg1*-null mice (7, 8). NDRG1 deficient mice also display impaired mast cell differentiation and degranulation (9). Despite numerous studies, including a particular emphasis on mechanisms of metastasis suppression (reviewed in (10)), the molecular function of NDRG1 remains elusive. While conserved peptide sequences place NDRG1 in the α/β hydrolase superfamily, there is no evidence of such enzymatic activity by this protein. Expression of NDRG1 is stimulated by multiple diverse signals, including tunicamycin (11), metals (cobalt, nickel, calcium and iron chelators) (12, 13), nitric oxide (14), vitamin D (15), vitamin C (16), retinoids (17), androgen and estrogen (18–21), and DNA damaging compounds (actinomycin D, doxorubicin, geldanamycin) (22–24). Several

ISSN Print 0013-7227 ISSN Online 1945-7170
Printed in U.S.A.

Received May 8, 2013. Accepted December 4, 2013.

Abbreviations:

prior findings implicate NDRG1 as relevant to cholesterol metabolism: (a) NDRG1 interacts with apolipoproteins A1 and A2, key proteins in HDL synthesis and reverse cholesterol transport (6), (b) humans with CMT4D mutations are affected with hypercholesterolemia and a sex-specific defect in reverse cholesterol transport (6, 25), and (c) the demyelinating phenotype of CMT4D mutation implicates NDRG1 in cholesterol metabolism, as high concentrations of cholesterol are required for myelin synthesis (26, 27).

Previous work in our lab demonstrated that NDRG1 is up-regulated in primary term human trophoblasts (PHT) cultured in hypoxia (28). Additionally, we and others have found increased expression of NDRG1 in placentas from pregnancies affected by FGR (29, 30). We also showed that overexpression of *NDRG1* in PHT cells enhances cell differentiation, while silencing of *NDRG1* potentiates hypoxia-induced apoptosis (31), suggesting that placental expression of NDRG1 constitutes an adaptive response to injury. Having found that NDRG1 bolstered differentiation and protected trophoblasts from hypoxic injury in vitro, we sought to test the hypothesis that NDRG1 is critical for placental function and fetal growth in vivo. We found that *Ndrg1* deletion in the mouse caused FGR and led to an increased rate of hypoxia-induced death of female, but not male, embryos. We also found that *Ndrg1* deletion caused significant alterations in placental gene expression, with a marked reduction in transcription of several lipoproteins in the placental labyrinth. These changes were associated with a female-specific reduction in the ratio of fetal:maternal serum cholesterol. Collectively, these findings indicate that (1) NDRG1 regulates the placental adaptive response to injury in vivo, (2) NDRG1 supports the maintenance of intrauterine cholesterol homeostasis, and (3) these effects are influenced by fetal sex.

Materials and Methods

Mouse breeding, genotyping and exposure to hypoxia

The Institutional Animal Care and Use Committee of the University of Pittsburgh approved our protocols. The generation of the *Ndrg1*-null mouse line was described by Okuda et al (8). Timed breeding of C57BL/6 mice heterozygous for the *Ndrg1*-null allele was performed by pairing heterozygous males and females overnight, with separation the next morning, designated as embryonic day 0.5 (E0.5). Pregnancy was assumed based on a weight gain of 10% or greater at E10.5. Mice were given standard chow and water ad libitum, and kept on a 12:12h light-dark cycle in room air. For hypoxia exposure, pregnant dams were placed in a Polymer Hypoxic Glove Box with a Purge Airlock system and CO_2 and O_2 control indicators (Coy Laboratory Products, Grass Lake, MI), designed for experiments in live rodents, with controlled and monitored humidity and gas composition. Exposure to hypoxia was initiated on E12.5, when fetal survival and growth definitively depends on placental function (32). The O_2 level was set at 12% for hypoxic animals (33), while normoxic controls remained in ambient air. Dams were sacrificed on E18.5 by cervical dislocation following isoflurane anesthesia. Embryos and placentas were immediately weighed, and tissues were subsequently processed for further analysis. Genomic DNA was extracted from embryo tails by the alkaline lysis and boiling method (34) and analyzed for *Ndrg1* genotype (8). Fetal sex was determined by PCR amplification of SRY (35).

In situ hybridization

To detect NDRG1 mRNA in tissues, we performed in situ hybridization, as previously published (36). Briefly, 10-μm frozen sections of OCT-embedded murine placentas were rehydrated, digested with proteinase K (Sigma, St. Louis, MO) at 10 μg/ml for 15 minutes at 37°C, treated with 0.2 N HCl for 10 minutes at room temperature, acetylated (0.25% acetic anhydride in triethanolamine for 10 minutes at room temperature), and then hybridized with cRNA probes overnight at 60°C. Slides were washed with saline-sodium citrate, digested with 20 μg/ml RNaseA (Sigma) for 30 minutes at 37°C, washed, and blocked using 1% blocking reagent (Roche, Manheim, Germany) in maleic acid buffer, followed by incubation with anti-DIG-AP antibody (Roche) at 0.5 U/ml for 2 hours at room temperature, washed, and then reacted with BM purple (Roche) with 1 mM levamisole overnight.

RNA isolation and RT-qPCR analysis

To extract RNA, we homogenized placental tissue using a T10 Basic S1 homogenizer (IKA Works, Wilmington, NC). Following homogenization, RNA for RT-qPCR was extracted from placental homogenates using Tri-Reagent (Molecular Research Center, Cincinnati, OH) according to the manufacturer's instruction. After removal of contaminating DNA using DNA-free (Invitrogen, Carlsbad, CA), extracted RNA was quantified using a NanoDrop-1000 spectrophotometer (Fisher-Thermo, Waltham, MA). 1 μg of RNA served as the template for reverse transcription (RT) using the SuperScript VILO kit (Invitrogen) according to the manufacturer's instructions. The RT product was diluted to a total volume of 100 μl, and 3 μl were used for PCR using 250 nM concentrations for forward and reverse gene-specific primers (Table 1) and SYBR Green PCR Master Mix (Applied Biosystems, Warrington, UK) in a total reaction volume of 10 μl. Reactions were run in duplicate and analyzed using an Applied Biosystems GeneAmp 7900 Sequence Detection System. Dissociation curves were run on all reactions, and samples were normalized to *L32* expression (37). Relative expression changes were calculated using the $\Delta\Delta$Ct method (38).

Western blot analysis

Western immunoblotting was performed as previously described (36). Proteins were extracted from placental tissue by homogenization in lysis buffer. Protein lysates were electrophoresed using 10% SDS-polyacrylamide gel at 130 V, then transferred to PVDF membranes (Biorad, Hercules, CA) at 23 V overnight. After blocking with 5% nonfat dried milk in Tris-buffered saline with 0.05% Tween-20, membranes were incubated over-

Table 1. Primers used for PCR

Transcript	Direction	Sequence
SRY	F	ATTTATGGTGTGGTCCCGTG
	R	AAGCTTTGCTGGTTTTTGGA
L32	F	CCTCTGGTGAAGCCCAAGATC
	R	TCTGGGTTTCCGCCAGTTT
Apoa1	F	GCTCAAGAGCAACCCTACCTT
	R	GCTTTCTCGCCAAGTGTCTTC
Apoa2	F	GCAGACGGACCGGATATGC
	R	GCTGCTCGTGTGTCTTCTCA
Apoa4	F	TCAGAAGACGGATGTCACTCA
	R	ATGCGGTCACGTAGGTCCT
Apoa5	F	TCCTCGCAGTGTTCGCAAG
	R	GAAGCTGCCTTTCAGGTTCTC
Apoc2	F	ACCTGTACCAGAAGACATACCC
	R	CCTGCGTAAGTGCTCATGG
Apoc4	F	TGTTCTTGGTCAGCTTTGTAGC
	R	AGGCTGTGGGTCTTGTTTAGG

night with rabbit anti-NDRG1 antibody (0.25 μg/mL, Invitrogen) at 4°C. The membranes were washed, and incubated with peroxidase conjugated goat antirabbit IgG (40 ng/mL, Santa Cruz Biotech, Santa Cruz, CA) for 2 hours at room temperature. Detection was performed with SuperSignal West Dura kit (Thermo Scientific, Rockford, IL).

Laser capture microdissection

10-μm frozen sections of OCT-embedded murine placentas were fixed on polyethylene naphthalate (PEN) membrane slides (Life Technologies, Carlsbad, CA) and stained with cresyl violet. Using the Leica CTR6500 laser capture microdissection system (Leica, Wetzlar, Germany), the placental labyrinth was visualized, circumscribed and collected by gravity-assisted microdissection. Following the collection of tissue, samples were immediately placed on ice. RNA was then extracted and qPCR performed as outlined above.

Cholesterol assay

Following sacrifice, maternal whole blood was collected by intracardiac aspiration. Fetal blood samples were obtained by collecting drained whole blood following decapitation. Whole blood from 152 embryos and 25 pregnant dams was heated to 37°C for 30 minutes to promote coagulation, and then stored at 4°C overnight. Samples were centrifuged at 1000 rpm for 10 minutes, and the supernatant serum was collected for analysis.

For quantification of placental cholesterol concentrations, we removed nonadherent decidual tissue from one-fourth of each placenta's basal plate. The remaining tissue was weighed, and homogenized in a glass tube using a Teflon pestle (Thomas Scientific, Swedesboro, NJ). Cholesterol was extracted from tissue for measurement with the Cholesterol Quantitation Kit (BioVision, Mountain View, CA), according to the manufacturers instructions, using a VersaMax microplate reader (Molecular Devices, Sunnyvale, CA). This assay relies on reference standards for establishment of optical density - concentration curves. All assays were performed in duplicate, with the coefficient of variation between duplicates consistently below 10%.

Statistics

Statistical analyses were performed using Stata (Stata, College Station, TX). ANOVA with post hoc Bonferroni correction for multiple comparisons was used to compare placenta and embryo weights across genotypes. The correlation between fetal serum cholesterol concentration and weight was quantified with the pairwise correlation coefficient. Genotype frequency distributions were compared using Fisher's exact test, and the χ^2 test was used to compare the proportion of specific gene categories in groups of differentially regulated transcripts following the microarray analysis. Gene expression was compared in WT and KO mice following RT-qPCR using Student's *t* test. Multivariate linear regression was used to compare fetal serum cholesterol levels across *Ndrg1* genotypes while controlling for the effect of fetal sex, hypoxia and litter size.

Results

NDRG1 is expressed in the mouse placenta

Whereas the expression of NDRG1 in the murine kidney and peripheral nerves has been previously validated (8), NDRG1's expression in the murine placenta has not been hitherto explored. Using in situ hybridization with adult mouse kidney as a positive control (Figure 1A), we found that *Ndrg1* was expressed in the mouse placenta, localized predominantly to the labyrinth and adjacent, maternally-derived uterine decidua, but not to the junctional zone (Figure 1B). These findings were confirmed using immunohistochemistry (not shown). In *Ndrg1*-null placentas derived from heterozygous dams, we detected *Ndrg1* expression in the decidua, as expected, but not in the fetal-derived placental tissue (Figure 1A, lower panel). We confirmed the expected level of RNA and protein expression in WT, heterozygote (Het) and KO placental homogenates using RT-qPCR and immunoblotting (Figure 1C-D).

NDRG1 deletion causes FGR

To investigate the effect of *Ndrg1* deletion on feto-placental development in vivo, we performed timed-breeding of heterozygous males and females and analyzed the offspring following sacrifice of pregnant dams on E18.5. KO embryos were growth restricted in comparison to WT and Het embryos (Figure 2A). We previously showed that silencing of endogenous *Ndrg1* in hypoxic PHT cells enhanced cell injury, and NDRG1 overexpression protected trophoblasts from hypoxic injury (31). To determine the effect of hypoxia on KO embryos, we placed pregnant dams in an atmosphere of 12% O_2 between E12.5 - E18.5, and compared fetal and placental weights across the different genotypes. Hypoxia caused a universal reduction in embryo weight ($P < .001$ by multivariable linear regression). Notably, when stratified by fetal sex, KO females

demonstrated a trend toward greatest weight reduction upon hypoxic exposure (Figure 2A, right panel). With the exception of male embryos bred in standard conditions, NDRG1 deficiency also caused a significant reduction in placental weight (Figure 2B). Additionally, in standard conditions the ratio of embryo:placenta weight was reduced in male KO embryos. Hypoxia caused a significant reduction of the embryo:placenta weight ratio in all strata, which was further exacerbated by *Ndrg1* deletion in female embryos (Figure 2C). While KO placentas were smaller, we found no significant effect of *Ndrg1* deletion on placental histologic morphology (not shown).

To determine if deletion of *Ndrg1* impacted intrauterine survival, we examined the genotype of all intact embryos on E18.5. Isolated placentas and partially resorbed embryos were not counted. In control litters exposed to room air, the genotypes of male and female progeny from heterozygous matings were distributed at the expected Mendelian frequency (Figure 3), indicating that loss of NDRG1 did not impact survival. However, with exposure to hypoxia,we observed a significant reduction in the number of female KO embryos that survived to E18.5 ($P < .01$, Fisher's exact test), with no effect in males, indicating that NDRG1 deficiency confers susceptibility to hypoxia-induced fetal death in a sex-dependent manner.

Ndrg1 deletion affects expression of placental apolipoproteins

Having shown that NDRG1 deficiency influences intrauterine growth and the fetal response to hypoxia, we sought to examine the expression changes of candidate genes that might contribute to the phenotype of NDRG1 deficient embryos. Notably, NDRG1 is known to interact with HDL-associated apolipoproteins and has been implicated in regulation of cholesterol metabolism and cellular stress response (5, 6, 25). We therefore focused on expression of key apolipoproteins involved in cholesterol transport and the response to oxidative stress (39–42). In order to identify transcriptional changes specifically associated with *Ndrg1* deletion, we performed laser capture microdissection to isolate tissue from the placental labyrinth, where *Ndrg1* expression was localized (Figure 1A). Figure 4 depicts changes in expression of major apolipoproteins in WT vs. KO placentas. In standard conditions, *Ndrg1* deletion had no significant effect on expression of these transcripts in the placental labyrinth. However, with exposure to hypoxia, NDRG1 deficiency led to reduced expression of *Apoa2*, *Apoa4*, *Apoa5*, *Apoc2* and *Apoc4*. Fetal sex had no effect on apolipoproteins in the labyrinth. .

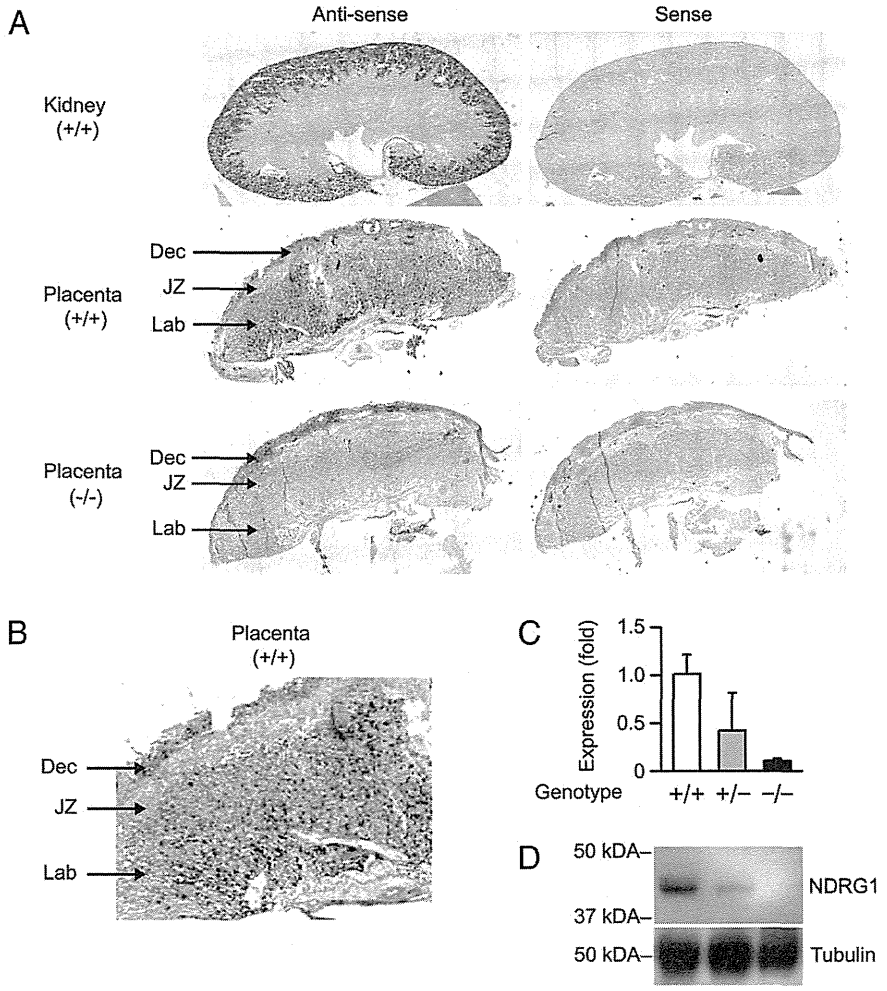

Figure 1. NDRG1 is expressed in WT and absent in KO mouse placentas; a) *In*-situ hybridization showing *Ndrg1* expression in WT adult kidney, WT placenta and KO placenta; b) *Ndrg1* expression in WT placenta; c) RT-qPCR showing expression of *Ndrg1* in WT, Het, and KO placenta (n = 3); d) Western immunoblot showing expression of NDRG1 in WT, Het, and KO placenta (representative of three experiments). Tubulin was used as a loading control. Dec, Decidua; JZ, Junctional zone; Lab, Labyrinth.

Fetal serum cholesterol is reduced in hypoxic *Ndrg1-null pups*

To determine if these changes in apolipoprotein expression were associated with altered feto-placental cholesterol levels, we measured total cholesterol in fetal and maternal serum. When normalized to maternal serum cholesterol, hypoxia caused a universal reduction in fetal serum

cholesterol levels ($P < .001$ by multivariable linear regression, Figure 5A). While the effect of hypoxia on fetal serum cholesterol was not influenced by NDRG1 in male embryos, female embryos displayed reduced relative cholesterol levels in KO embryos compared to WT or Het animals ($P = .001$). Notably, despite differences in serum cholesterol levels, we found no difference in the amount of cholesterol accumulated in placental tissue stemming from differences in sex, oxygen level, or *Ndrg1* expression (Figure 5B). Finally, fetal serum cholesterol levels were positively correlated with fetal weight (Figure 5C; pairwise correlation coefficient 0.2542, $P = .0016$).

Discussion

Our findings establish the pregnancy-related phenotype of NDRG1 deficiency, demonstrating fetal growth restriction stemming from *Ndrg1* deletion, and support our prior in vitro findings of a protective role for NDRG1 in the maintenance of placental function (31). *Ndrg1* is expressed in the murine placental labyrinth, the region that mediates maternal-fetal exchange and is largely analogous to human synctiotrophoblasts. These data, coupled with the increased expression of NDRG1 in hypoxic trophoblasts and placentas from pregnancies complicated by FGR (28–31), further support the conclusion that increased placental expression of NDRG1 constitutes an adaptive response to hypoxic injury. Future experiments using Cre recombinase to specifically delete a floxed *Ndrg1* allele in the embryo or placenta will distinguish the relative contribution of fetal vs. placental gene deletion to the observed phenotype.

Placental metabolism, steroid processing, and perinatal outcomes are largely influenced by fetal sex (44–48). In the human placenta, gene expression diverges according to sex (49) and, in mice, the response to environmental exposures, such as fat content in maternal diet, impacts placental gene expression and intrauterine survival in a sexually dichotomous manner (44, 50). The Liver X Receptor (LXR) is a key transcriptional regulator of cholesterol metabolism and regulates the transcription of the ApoE/C-I/C-IV/C-II gene cluster (42, 51, 52). Functional crosstalk between the Liver X Receptor and sex steroid receptors has been demonstrated to influence cholesterol metabolism (53). Of relevance, the LXRβ-deficient mouse displays motor neuron degeneration exclusively in males and NDRG1-null humans affected with Charcot-Marie-Tooth 4D demonstrate a male-specific reduction in serum HDL (6, 53). Differences in circulating sex hormone concentrations and/or receptor expression may contribute to the sex differences in hypoxia-induced mortality and serum cholesterol that we observed in hypoxic KO animals. Alternatively, sexually discrepant regulation of genes on the X chromosome may underlie the observed phenotypic differences. The escape of specific genes from X chromosome inactivation in females can be affected by environmental stressors including hypoxia, and is differentially regulated in spe-

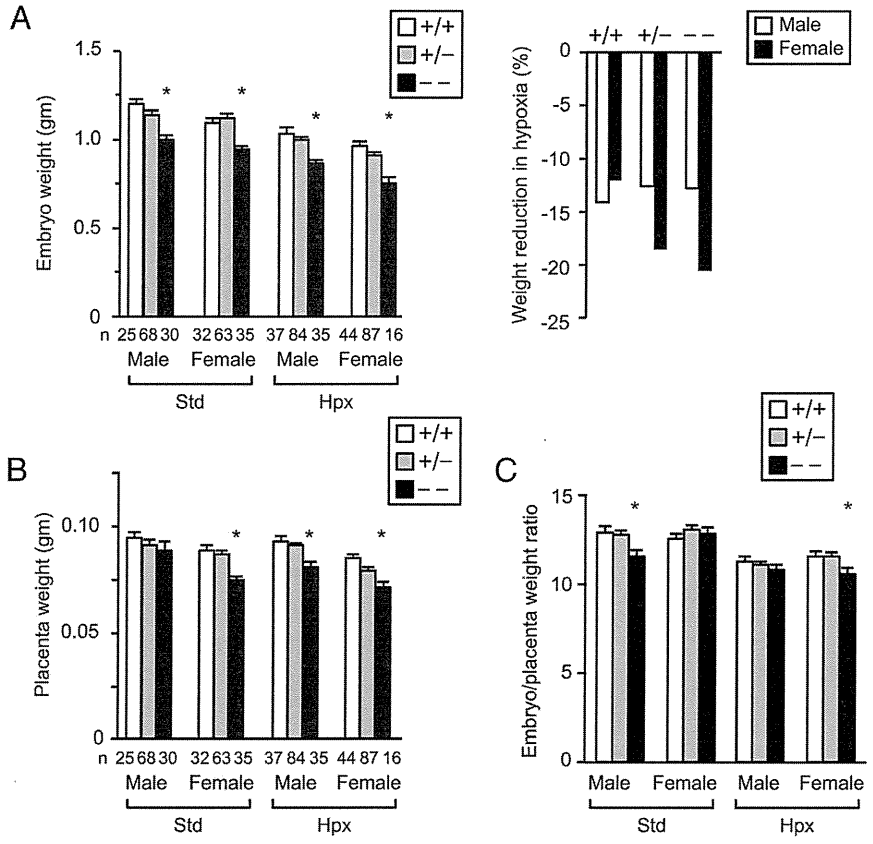

Figure 2. *Ndrg1* deletion causes fetal growth restriction and reduced placental weight; a) Mean embryo weight (gm) at E18.5, stratified by sex, genotype and O_2 level (Left); Reduction in fetal weight resulting from exposure to hypoxia, stratified by fetal sex and genotype (Right); b) Mean placenta weight (gm) at E18.5, stratified by fetal sex, genotype and O_2 level; c) Mean ratio of embryo:placenta weight at E18.5. *$P < .05$ compared to WT of same sex and oxygen level by ANOVA with Bonferroni correction; Hypoxia (Hpx) denotes placement of pregnant dams in 12% O_2 between E12.5 and E18.5, and compared to standard (Std) conditions. The numbers (n) below the bars denote the number of embryos analyzed for each paradigm. Note also that hypoxia caused a universal reduction in embryo weight and embryo:placenta weight ratio ($P <$ .001 by multivariable linear regression).

cific extraembryonic cell lineages (54–56). Hypoxia and/or NDRG1 deficiency may lead to female-specific alterations in expression of X chromosome genes that are maladaptive with exposure to a second insult, causing exacerbation of injury specifically in female, *Ndrg1*-null, hypoxic embryos. Our data indicate that the phenotypic differences in the effect of NDRG1 deficiency in male and female embryos do not stem from differences in apolipoprotein expression, as transcription of apolipoproteins was comparably affected by *Ndrg1* deletion and hypoxia in the labyrinth of male and female placentas.

We demonstrated that hypoxic injury reduces fetal cholesterol serum levels, and that this reduction is exacerbated by NDRG1 deficiency in females. The change we observed in fetal:maternal serum cholesterol ratio was not mediated by the accumulation of cholesterol in the placenta, as placental cholesterol levels were unchanged with hypoxia or *Ndrg1* deletion. This finding suggests that fetal cholesterol decreased as a result of a reduction in either net cholesterol uptake from the maternal circulation or reduced de novo fetal cholesterol synthesis, and highlights the need for further insight into maternal-fetal cholesterol trafficking.

There is a well-established association between FGR, lipid peroxidation and hypocholesterolemia (57–59). Tissue hypoxia precipitates accumulation of reactive oxygen species, which promotes the unregulated oxidation of cholesterol and LXR activation (60–62). Thus, it is likely that placental hypoperfusion and hypoxia, critical mediators of FGR, contribute to the associated derangements in cholesterol metabolism. The placental metabolic response to uncontrolled cholesterol oxidation and/or hypoxic injury may promote trophoblast survival at the expense of fetal nutrient delivery and growth. Our findings implicate NDRG1 as a regulator of this response, and highlight the negative effect of disrupted cholesterol metabolism on intrauterine growth and development.

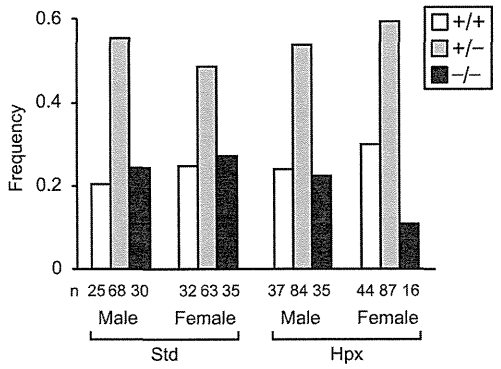

Figure 3. *Ndrg1* deletion causes hypoxia-induced intrauterine death in female embryos; genotype frequencies following stratification by O_2 level and fetal sex. Genotype frequencies deviated from expected Mendelian frequency exclusively in hypoxic females ($P < .01$, Fisher's exact test). The numbers (n) below the bars denote the number of embryos analyzed for each paradigm. Standard (Std) and Hypoxia (Hpx) conditions are as described in Figure 2.

Acknowledgments

We thank Tianjiao Chu for analysis and advice regarding statistics, Patrick Reidy, Elena Sadovsky and Huijie Sun for technical assistance, and Lori Rideout for assistance with manuscript preparation.

Address all correspondence and requests for reprints to: Yoel Sadovsky, MD, Magee-Womens Research Institute, 204 Craft Avenue, Pittsburgh, PA 15213, Ph 412–641-2675 / Fx 412–641-3898, Email ysadovsky@mwri.magee.edu

Reprints: Will not be available.

Disclosure: The authors have nothing to disclose.

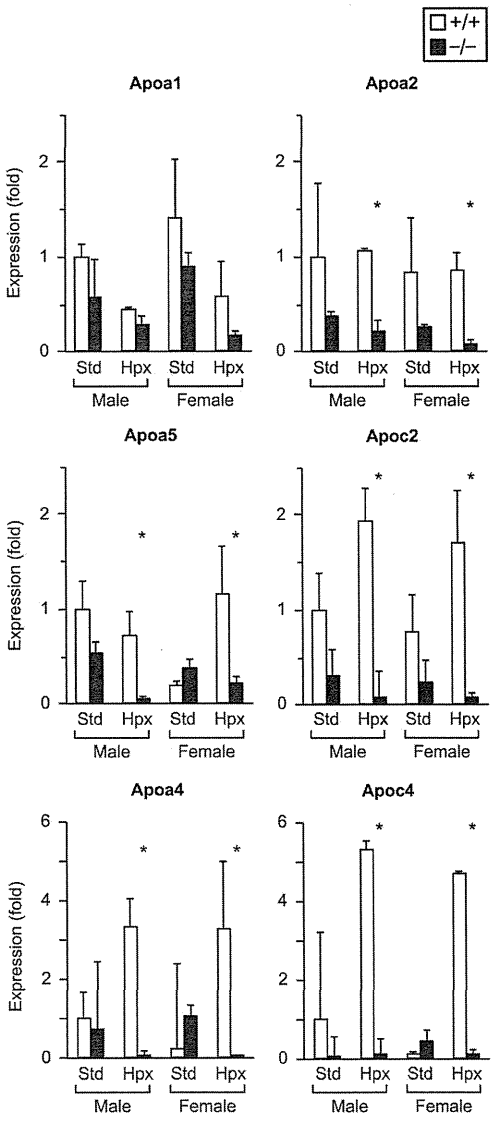

Figure 4. The impact of *Ndrg1* deletion on apolipoprotein expression in the placental labyrinth; RT-qPCR results (n = 2–4, each group); $*P < .05$ by Student's two-tailed *t* test in WT vs. KO of same sex at same oxygen level.

This work was supported by **Financial support:** This project is supported by a grant from the American Association of OB-GYN Foundation/Society for Maternal-Fetal Medicine (JL), PA Department of Health Research Formula Funds (JL), NIH grants K12HD063087 (JL), P01 HD069316 (YS and YB), R01 HD045675 (YS), and R01 ES011597 (YS).

References

1. **Resnik R.** Intrauterine growth restriction. *Obstet Gynecol.* 2002; 99:490–496.
2. **Barker DJ.** Fetal growth and adult disease. *Br J Obstet Gynaecol.* 1992;99:275–276.
3. **McIntire DD, Bloom SL, Casey BM, Leveno KJ.** Birth weight in relation to morbidity and mortality among newborn infants. *N Engl J Med.* 1999;340:1234–1238.
4. **Bernstein IM, Horbar JD, Badger GJ, Ohlsson A, Golan A.** Morbidity and mortality among very-low-birth-weight neonates with intrauterine growth restriction. The Vermont Oxford Network. *Am J Obstet Gynecol.* 2000;182:198–206.
5. **Kachhap SK, Faith D, Qian DZ, Shabbeer S, Galloway NL, Pili R, Denmeade SR, DeMarzo AM, Carducci MA.** The N-Myc down regulated Gene1 (NDRG1) Is a Rab4a effector involved in vesicular recycling of E-cadherin. *PLoS ONE.* 2007;2:e844.
6. **Hunter M, Angelicheva D, Tournev I, Ingley E, Chan DC, Watts GF, Kremensky I, Kalaydjieva L.** NDRG1 interacts with APO A-I and A-II and is a functional candidate for the HDL-C QTL on 8q24. *Biochem Biophys Res Commun.* 2005;332:982–992.
7. **Kalaydjieva L, Gresham D, Gooding R, Heather L, Baas F, de Jonge R, Blechschmidt K, Angelicheva D, Chandler D, Worsley P, Rosenthal A, King RH, Thomas PK.** N-myc downstream-regulated gene 1 is mutated in hereditary motor and sensory neuropathy-Lom. *Am J Hum Genet.* 2000;67:47–58.
8. **Okuda T, Higashi Y, Kokame K, Tanaka C, Kondoh H, Miyata T.** Ndrg1-deficient mice exhibit a progressive demyelinating disorder of peripheral nerves. *Molecular and cellular biology.* 2004;24: 3949–3956.
9. **Taketomi Y, Sunaga K, Tanaka S, Nakamura M, Arata S, Okuda T, Moon TC, Chang HW, Sugimoto Y, Kokame K, Miyata T, Murakami M, Kudo I.** Impaired mast cell maturation and degranulation and attenuated allergic responses in Ndrg1-deficient mice. *J Immunol.* 2007;178:7042–7053.
10. **Ellen TP, Ke Q, Zhang P, Costa M.** NDRG1, a growth and cancer related gene: regulation of gene expression and function in normal and disease states. *Carcinogenesis.* 2008;29:2–8.
11. **Kokame K, Kato H, Miyata T.** Homocysteine-respondent genes in vascular endothelial cells identified by differential display analysis. GRP78/BiP and novel genes. *J Biol Chem.* 1996;271:29659–29665.
12. **Le NT, Richardson DR.** Iron chelators with high antiproliferative activity up-regulate the expression of a growth inhibitory and metastasis suppressor gene: a link between iron metabolism and proliferation. *Blood.* 2004;104:2967–2975.
13. **Chen Z, Zhang D, Yue F, Zheng M, Kovacevic Z, Richardson DR.** The iron chelators Dp44mT and DFO inhibit TGF-beta-induced epithelial-mesenchymal transition via up-regulation of N-Myc downstream-regulated gene 1 (NDRG1). *J Biol Chem.* 287:17016–17028.
14. **Hickok JR, Sahni S, Mikhed Y, Bonini MG, Thomas DD.** Nitric oxide suppresses tumor cell migration through N-Myc downstream-regulated gene-1 (NDRG1) expression: role of chelatable iron. *J Biol Chem.* 286:41413–41424.
15. **Matsugaki T, Zenmyo M, Hiraoka K, Fukushima N, Shoda T, Komiya S, Ono M, Kuwano M, Nagata K.** N-myc downstream-regulated gene 1/Cap43 expression promotes cell differentiation of human osteosarcoma cells. *Oncol Rep.* 24:721–725.
16. **Karaczyn A, Ivanov S, Reynolds M, Zhitkovich A, Kasprzak KS, Salnikow K.** Ascorbate depletion mediates up-regulation of hypoxia-associated proteins by cell density and nickel. *J Cell Biochem.* 2006;97:1025–1035.
17. **Chen S, Han YH, Zheng Y, Zhao M, Yan H, Zhao Q, Chen GQ, Li D.** NDRG1 contributes to retinoic acid-induced differentiation of leukemic cells. *Leuk Res.* 2009;33:1108–1113.
18. **Mostaghel EA, Page ST, Lin DW, Fazli L, Coleman IM, True LD, Knudsen B, Hess DL, Nelson CC, Matsumoto AM, Bremner WJ, Gleave ME, Nelson PS.** Intraprostatic androgens and androgen-regulated gene expression persist after testosterone suppression: therapeutic implications for castration-resistant prostate cancer. *Cancer Res.* 2007;67:5033–5041.
19. **Pflueger D, Rickman DS, Sboner A, Perner S, LaFargue CJ, Svensson MA, Moss BJ, Kitabayashi N, Pan Y, de la Taille A, Kuefer R, Tewari AK, Demichelis F, Chee MS, Gerstein MB, Rubin MA.** N-

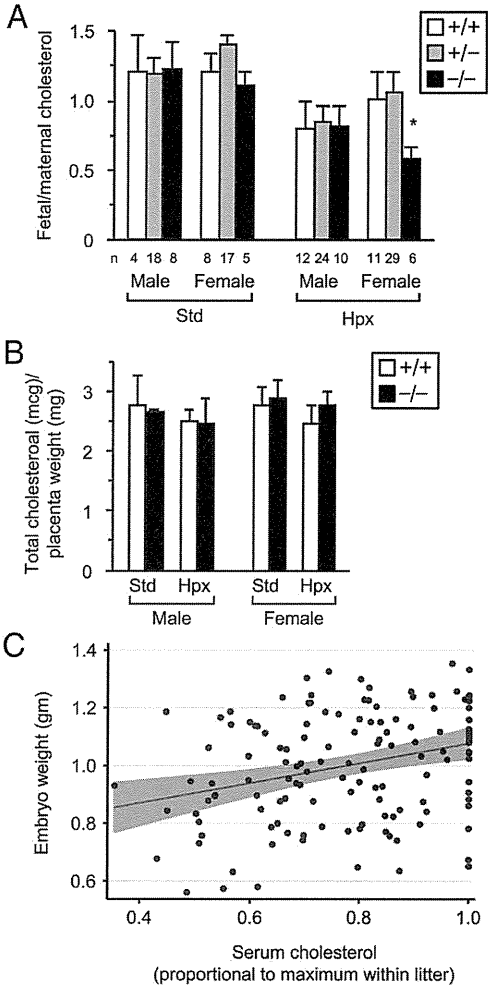

Figure 5. NDRG1 deficiency modulates fetal serum cholesterol a) Mean fetal:maternal ratio of serum cholesterol concentration; *P = .001 by Student's t test compared to WT and Het. Note also that hypoxia caused a universal reduction in fetal:maternal serum cholesterol ratio ($P < .001$ by multivariable linear regression). The numbers (n) below the bars denote the number of embryos analyzed of reach paradigm. Standard (Std) and Hypoxia (Hpx) conditions are as described in Figure 2; b) Total cholesterol content in placental tissue (n = 3). Standard (Std) and Hypoxia (Hpx) conditions are as described in Figure 2; c) Fetal serum cholesterol (proportional to maximum value within litter) correlates with embryo weight; pairwise correlation coefficient 0.2542, $P = .0016$.

myc downstream regulated gene 1 (NDRG1) is fused to ERG in prostate cancer. *Neoplasia.* 2009;11:804–811.
20. **Fotovati A, Fujii T, Yamaguchi M, Kage M, Shirouzu K, Oie S, Basaki Y, Ono M, Yamana H, Kuwano M.** 17Beta-estradiol induces down-regulation of Cap43/NDRG1/Drg-1, a putative differentiation-related and metastasis suppressor gene, in human breast cancer cells. *Clin Cancer Res.* 2006;12:3010–3018.
21. **Fujii T, Yokoyama G, Takahashi H, Toh U, Kage M, Ono M, Shirouzu K, Kuwano M.** Preclinical and clinical studies of novel breast cancer drugs targeting molecules involved in protein kinase C signaling, the putative metastasis-suppressor gene Cap43 and the Y-box binding protein-1. *Curr Med Chem.* 2008;15:528–537.
22. **Xu X, Sutak R, Richardson DR.** Iron chelation by clinically relevant anthracyclines: alteration in expression of iron-regulated genes and atypical changes in intracellular iron distribution and trafficking. *Mol Pharmacol.* 2008;73:833–844.
23. **Banz VM, Medova M, Keogh A, Furer C, Zimmer Y, Candinas D, Stroka D.** Hsp90 transcriptionally and post-translationally regulates the expression of NDRG1 and maintains the stability of its modifying kinase GSK3beta. *Biochim Biophys Acta.* 2009;1793: 1597–1603.
24. **Jung EU, Yoon JH, Lee YJ, Lee JH, Kim BH, Yu SJ, Myung SJ, Kim YJ, Lee HS.** Hypoxia and retinoic acid-inducible NDRG1 expression is responsible for doxorubicin and retinoic acid resistance in hepatocellular carcinoma cells. *Cancer Lett.* 298:9–15.
25. **Dackovic J, Keckarevic-Markovic M, Komazec Z, Rakocevic-Stojanovic V, Lavrnic D, Stevic Z, Ribaric K, Romac S, Apostolski S.** Hereditary motor and sensory neuropathy Lom type in a Serbian family. *Acta myologica : myopathies and cardiomyopathies : official journal of the Mediterranean Society of Myology / edited by the Gaetano Conte Academy for the study of striated muscle diseases.* 2008;27:59–62.
26. **Verheijen MH, Camargo N, Verdier V, Nadra K, de Preux Charles AS, Medard JJ, Luoma A, Crowther M, Inouye H, Shimano H, Chen S, Brouwers JF, Helms JB, Feltri ML, Wrabetz L, Kirschner D, Chrast R, Smit AB.** SCAP is required for timely and proper myelin membrane synthesis. *Proc Natl Acad Sci U S A.* 2009;106:21383–21388.
27. **Saher G, Brugger B, Lappe-Siefke C, Mobius W, Tozawa R, Wehr MC, Wieland F, Ishibashi S, Nave KA.** High cholesterol level is essential for myelin membrane growth. *Nat Neurosci.* 2005;8:468–475.
28. **Roh CR, Budhraja V, Kim HS, Nelson DM, Sadovsky Y.** Microarray-based identification of differentially expressed genes in hypoxic term human trophoblasts and in placental villi of pregnancies with growth restricted fetuses. *Placenta.* 2005;26:319–328.
29. **Choi SJ, OH SY, Kim JH, Sadovsky Y, Roh CR 2007 Increased expression of N-myc downstream-regulated gene 1 (NDRG1) in placentas from pregnancies complicated by intrauterine growth restriction or preeclampsia.** *Am J Obstet Gynecol* 196:45 e41–47.
30. **Gratton RJ, Gluszynski M, Nygard K, Mazzuca DM, Graham CH, Han VK.** Reducing agent and tunicamycin-responsive protein (RTP) mRNA expression in the placentae of normal and pre-eclamptic women. *Placenta.* 2004;25:62–69.
31. **Chen B, Nelson DM, Sadovsky Y.** N-myc down-regulated gene 1 modulates the response of term human trophoblasts to hypoxic injury. *J Biol Chem.* 2006;281:2764–2772.
32. **Barak Y, Nelson MC, Ong ES, Jones YZ, Ruiz-Lozano P, Chien KR, Koder A, Evans RM.** PPAR gamma is required for placental, cardiac, and adipose tissue development. *Mol Cell.* 1999;4:585–595.
33. **Tomlinson TM, Garbow JR, Anderson JR, Engelbach JA, Nelson DM, Sadovsky Y.** Magnetic resonance imaging of hypoxic injury to the murine placenta. *Am J Physiol Regul Integr Comp Physiol.* 2010;298:R312–319.
34. **Hanley T, Merlie JP.** Transgene detection in unpurified mouse tail DNA by polymerase chain reaction. *BioTechniques.* 1991;10:56.
35. **Pomp D, Good BA, Geisert RD, Corbin CJ, Conley AJ.** Sex identification in mammals with polymerase chain reaction and its use to examine sex effects on diameter of day-10 or -11 pig embryos. *Journal of animal science.* 1995;73:1408–1415.
36. **Mishima T, Miner JH, Morizane M, Stahl A, Sadovsky Y.** The expression and function of fatty acid transport protein-2 and -4 in the murine placenta. *PLoS One.* 2011;6:e25865.
37. **Maity A, Solomon D.** Both increased stability and transcription contribute to the induction of the urokinase plasminogen activator receptor (uPAR) message by hypoxia. *Experimental cell research.* 2000;255:250–257.
38. **Livak KJ, Schmittgen TD.** Analysis of relative gene expression data using real-time quantitative PCR and the 2(-Delta Delta C(T)) Method. *Methods.* 2001;25:402–408.
39. **Qin X, Swertfeger DK, Zheng S, Hui DY, Tso P.** Apolipoprotein AIV: a potent endogenous inhibitor of lipid oxidation. *The American journal of physiology.* 1998;274:H1836–1840.
40. **Duka A, Fotakis P, Georgiadou D, Kateifides A, Tzavlaki K, von Eckardstein L, Stratikos E, Kardassis D, Zannis VI.** ApoA-IV promotes the biogenesis of apoA-IV-containing HDL particles with the participation of ABCA1 and LCAT. *J Lipid Res.* 2013;54:107–115.
41. **Soran H, Hama S, Yadav R, Durrington PN.** HDL functionality. *Current opinion in lipidology.* 2012;23:353–366.
42. **Mak PA, Laffitte BA, Desrumaux C, Joseph SB, Curtiss LK, Mangelsdorf DJ, Tontonoz P, Edwards PA.** Regulated expression of the apolipoprotein E/C-I/C-IV/C-II gene cluster in murine and human macrophages. A critical role for nuclear liver X receptors alpha and beta. *J Biol Chem.* 2002;277:31900–31908.
43. **Hayashi S, Lewis P, Pevny L, McMahon AP.** Efficient gene modulation in mouse epiblast using a Sox2Cre transgenic mouse strain. *Mech Dev.* 2002;119 Suppl 1:S97–S101.
44. **Rosenfeld CS, Grimm KM, Livingston KA, Brokman AM, Lamberson WE, Roberts RM.** Striking variation in the sex ratio of pups born to mice according to whether maternal diet is high in fat or carbohydrate. *Proc Natl Acad Sci U S A.* 2003;100:4628–4632.
45. **Andoh T, Uda H, Yoshimitsu N, Hatano H, Ueda T, Iwamatsu Y, Akiba S.** The sex differences in cord-blood cholesterol and fatty-acid levels among Japanese fetuses. *Journal of epidemiology / Japan Epidemiological Association.* 1997;7:226–231.
46. **Hagemenas FC, Kittinger GW.** The effect of fetal sex on placental biosynthesis of progesterone. *Endocrinology.* 1974;94:922–924.
47. **Sathishkumar K, Balakrishnan M, Chinnathambi V, Chauhan M, Hankins GD, Yallampalli C.** Fetal sex-related dysregulation in testosterone production and their receptor expression in the human placenta with preeclampsia. *Journal of perinatology : official journal of the California Perinatal Association.* 2012;32:328–335.
48. **Clifton VL.** Review: Sex and the human placenta: mediating differential strategies of fetal growth and survival. *Placenta.* 2010;31 Suppl:S33–39.
49. **Sood R, Zehnder JL, Druzin ML, Brown PO.** Gene expression patterns in human placenta. *Proc Natl Acad Sci U S A.* 2006;103:5478–5483.
50. **Mao J, Zhang X, Sieli PT, Falduto MT, Torres KE, Rosenfeld CS.** Contrasting effects of different maternal diets on sexually dimorphic gene expression in the murine placenta. *Proc Natl Acad Sci U S A.* 107:5557–5562.
51. **Zhang Y, Breevoort SR, Angdisen J, Fu M, Schmidt DR, Holmstrom SR, Kliewer SA, Mangelsdorf DJ, Schulman IG.** Liver LXRalpha expression is crucial for whole body cholesterol homeostasis and reverse cholesterol transport in mice. *The Journal of clinical investigation.* 2012;122:1688–1699.
52. **Tontonoz P, Mangelsdorf DJ.** Liver X receptor signaling pathways in cardiovascular disease. *Mol Endocrinol.* 2003;17:985–993.
53. **Andersson S, Gustafsson N, Warner M, Gustafsson JA.** Inactivation of liver X receptor beta leads to adult-onset motor neuron degeneration in male mice. *Proc Natl Acad Sci U S A.* 2005;102:3857–3862.
54. **Yang SY, Dobkin C, He XY, Brown WT** Transcription start sites

and epigenetic analysis of the HSD17B10 proximal promoter. *BMC biochemistry*. 2013;14:17.

55. **Corbel C, Diabangouaya P, Gendrel AV, Chow JC, Heard E.** Unusual chromatin status and organization of the inactive X chromosome in murine trophoblast giant cells. *Development*. 2013;140: 861–872.
56. **Du Yan S, Zhu Y, Stern ED, Hwang YC, Hori O, Ogawa S, Frosch MP, Connolly ES, Jr., McTaggert R, Pinsky DJ, Clarke S, Stern DM, Ramasamy R.** Amyloid beta -peptide-binding alcohol dehydrogenase is a component of the cellular response to nutritional stress. *J Biol Chem*. 2000;275:27100–27109.
57. **Leduc L, Delvin E, Ouellet A, Garofalo C, Grenier E, Morin L, Dube J, Bouity-Voubou M, Moutquin JM, Fouron JC, Klam S, Levy E.** Oxidized low-density lipoproteins in cord blood from neonates with intra-uterine growth restriction. *Eur J Obstet Gynecol Reprod Biol*. 2011;156:46–49.
58. **Spencer JA, Chang TC, Crook D, Proudler A, Felton CV, Robson SC, Hauesler M.** Third trimester fetal growth and measures of carbohydrate and lipid metabolism in umbilical venous blood at term. *Arch Dis Child Fetal Neonatal Ed*. 1997;76:F21–25.
59. **Pecks U, Brieger M, Schiessl B, Bauerschlag DO, Piroth D, Bruno B, Fitzner C, Orlikowsky T, Maass N, Rath W.** Maternal and fetal cord blood lipids in intrauterine growth restriction. *J Perinat Med*. 2012; 40:287–296.
60. **Miyata T, Takizawa S, van Ypersele de Strihou C.** Hypoxia. 1. Intracellular sensors for oxygen and oxidative stress: novel therapeutic targets. *American journal of physiology Cell physiology*. 2011;300:C226–231.
61. **Brown AJ, Jessup W.** Oxysterols: Sources, cellular storage and metabolism, and new insights into their roles in cholesterol homeostasis. *Molecular aspects of medicine*. 2009;30:111–122.
62. **Lehmann JM, Kliewer SA, Moore LB, Smith-Oliver TA, Oliver BB, Su JL, Sundseth SS, Winegar DA, Blanchard DE, Spencer TA, Willson TM.** Activation of the nuclear receptor LXR by oxysterols defines a new hormone response pathway. *J Biol Chem*. 1997;272: 3137–3140.

J. Biochem. 2013;154(1):41–50 doi:10.1093/jb/mvt024

JB THE JOURNAL OF BIOCHEMISTRY

Molecular mechanisms of syndecan-4 upregulation by TNF-α in the endothelium-like EAhy926 cells

Received November 19, 2012; accepted March 12, 2013; published online April 9, 2013

Eriko Okuyama[1], Atsuo Suzuki[1], Moe Murata[1], Yumi Ando[1], Io Kato[1], Yuki Takagi[1], Akira Takagi[1], Takashi Murate[1], Hidehiko Saito[2] and Tetsuhito Kojima[1,*]

[1]Department of Pathophysiological Laboratory Sciences, Nagoya University Graduate School of Medicine, Nagoya 461-8673; and [2]National Hospital Organization-Nagoya Medical Center, Nagoya 460-0001, Japan

*Tetsuhito Kojima, Department of Pathophysiological Laboratory Sciences, Nagoya University Graduate School of Medicine, 1-1-20 Daiko-Minami, Higashi-ku, Nagoya 461-8673, Japan. Tel:/Fax: +81-52-719-3153, email: kojima@met.nagoya-u.ac.jp

Syndecan-4, a cell-surface heparan sulfate proteoglycan, can participate in inflammation and wound healing as a host defense molecule. Tumour necrosis factor (TNF)-α, one of the most potent proinflammatory cytokines, is known to upregulate syndecan-4 expression, but the precise mechanisms are unclear. To elucidate these mechanisms in detail, we examined syndecan-4 upregulation by TNF-α in the endothelium-like EAhy926 cell. Of the two putative nuclear factor kappa-B (NF-κB) binding sites in the syndecan-4 gene (*SDC4*) promoter, deletion or mutation of one or both sites significantly diminished the effects of TNF-α. Electrophoretic mobility shift assays showed that p65 and c-Rel, but not p50, bound to these NF-κB binding sites, whereas pull-down assays showed binding of all three NF-κB components. Chromatin immunoprecipitation assays clearly showed that p65 and phosphorylated p65, but not p50 or c-Rel, bound to the *SDC4* promoter. An NF-κB inhibitor, p65 knockdown and a transcriptional elongation inhibitor completely blocked the effect of TNF-α on *SDC4* promoter activity and significantly, but not completely, blocked that on *SDC4* mRNA expression. These data suggest that NF-κB p65 could be a key mediator of syndecan-4 upregulation by TNF-α through two binding sites in the *SDC4* promoter, but other NF-κB-p65 independent pathways might also be involved through transcriptional elongation.

Keywords: NF-κB/p65/syndecan-4/TNF-α/upregulation.

Abbreviations: CDK9, cyclin-dependent kinase 9; ChIP, chromatin immunoprecipitation; DRB, 5,6-dichlorobenzimidazole-1-b-D-ribofuranoside; EMSA, electrophoretic mobility shift assay; IκB, inhibitor of kappa-B; NF-κB, nuclear factor kappa-B; P-TEFb, positive transcription elongation factor b; PBS, phosphate-buffered saline; siRNA, small interfering RNA; SDC4, syndecan-4; TNF-α, tumour necrosis factor-α.

Syndecan-4 is a member of the syndecan family of heparan sulfate proteoglycans and is expressed on the cell surface of various cell types including endothelial, epithelial and smooth muscle cells. Syndecan-4, also known as ryudocan, was originally isolated from endothelial cells as an anticoagulant molecule (*1*, *2*), but recently has been suggested to be involved in multiple biological functions (*3*). The syndecans including syndecan-4 selectively bind to various matrix components, growth factors and anticoagulant proteins through heparan sulfate glycosaminoglycan chains, and these interactions may facilitate important biological activities (*4*). Our recent studies using syndecan-4-deficient mice showed that syndecan-4 had a crucial role in preventing endotoxin shock, pulmonary inflammation and cardiac rupture after myocardial infarction, as well as in neointimal formation after vascular injury. Together, these data suggest that syndecan-4 could be an important molecule in host defense mechanisms by regulating inflammation, wound healing and tissue remodelling (*5–8*).

Tumour necrosis factor (TNF)-α is a major pro-inflammatory cytokine secreted predominantly by monocytes and macrophages. Previous studies have shown that TNF-α induced expression of pro-inflammatory cytokines and adhesion molecules in endothelial cells that is dependent on nuclear factor kappa-B (NF-κB) activation (*9*). Members of the NF-κB family of transcription factors are central mediators of immune, inflammatory and anti-apoptotic responses (*10*). NF-κB is activated in response to a broad range of extracellular signals including bacterial products, inflammatory cytokines and chemotherapeutic agents (*11*). A major pathway-regulating NF-κB activity involves its nuclear transport. In quiescent cells, NF-κB is retained in the cytoplasm in an inactivated form bound to its inhibitory proteins, known as inhibitor of kappa-B (IκBs). In response to cellular stimulations, IκBs are phosphorylated, ubiquitinated and subsequently degraded by the 26S proteasome (*12*). Then, NF-κB translocates to the nucleus and activates transcription of genes involved in immune functions and inflammatory responses.

Previous studies indicated that syndecan-4 expression increased after tissue injury (*7*, *8*), ischaemia (*13*) or bacterial infection (*14*, *15*). Furthermore, these studies demonstrated that syndecan-4 expression was enhanced by TNF-α, which was produced in response to hypoxic condition in the myocytes and *Helicobacter pylori* gastritis in the gastric mucosa. However, these studies did not evaluate the detailed regulation mechanisms underlying syndecan-4 expression. In this study, we investigated the molecular mechanisms of

syndecan-4 upregulation by TNF-α in EAhy926 cells, a human vascular endothelium-like cell line.

Materials and Methods

Cell culture

EAhy926 cells, a hybrid of a human umbilical vein endothelial cell and a lung carcinoma cell, were generously donated by Dr Cora-Jean S. Edgell (University of North Carolina, Chapel Hill, NC, USA) and maintained at 37°C and 5% CO_2 in Dulbecco's modified Eagle's medium (DMEM; WAKO, Tokyo, Japan), supplemented with 10% foetal bovine calf serum (FBS; JRH Biosciences, Lenexa, KS, USA) and 100× antibiotics–antimycotics mixed stock solution (Nacalai Tesque, Kyoto, Japan). Recombinant human TNF-α (Invitrogen, Carlsbad, CA, USA) was added to culture media to achieve a final concentration of 10 ng/ml. For the NF-κB inhibition study, cells were treated with 10 μM BAY11-7082 ((E)3-[(4-methylphenyl)-sulphonyl]-2-propenenitrile) (Calbiochem, SanDiego, CA, USA) for 1 h before TNF-α treatment. To verify the effects of transcriptional elongation on syndecan-4 expression induced by TNF-α, cells were pretreated with 50 μM 5,6-dichlorobenzimidazole-1-b-D-ribofuranoside (DRB) (Sigma-Aldrich, Saint Louis, MO, USA) for 1 h before TNF-α treatment.

Flow cytometry analysis

After 3 h of treatment with TNF-α or fresh media, EAhy926 cells were incubated for another 6 h and harvested from the plates using phosphate-buffered saline (PBS) containing 1 mM EDTA. The cells (1.2×10^5 cells) were stained with anti-syndecan-4 antibody [anti-Ryu2 antibody (*3*)] or normal rabbit IgG (Santa Cruz Biotechnology Inc., Santa Cruz, CA, USA) for 20 min at room temperature in PBS containing 1% FBS and 0.05% NaN_3. After washing, the cells were incubated with Alexa Fluor 488-conjugated goat anti-rabbit IgG (H+L) antibody (Invitrogen) for 20 min at room temperature and analysed using a FACS Calibur (BD Bioscience, Franklin Lakes, NJ, USA).

Quantitative reverse transcription-PCR

Total RNA from EAhy926 cells was isolated using an RNeasy Mini Kit (Qiagen, Hilden, Germany). The isolated RNA (750 ng) was used for cDNA synthesis using the Prime Script RT Master Mix (TaKaRa, Shiga, Japan). Quantitative reverse transcription (RT)-PCR was performed with SYBR Premix Ex Taq II (TaKaRa), and Thermal Cycler Dice Real Time System II (TaKaRa) was used for measurement. The following primers were used: *SDC4*, 5′-CTGGCTCTGGAGATCTGGATG-3′ and 5′-GTTTCTTGGGTTCGGTGGG-3′ and *GUSB* (beta-glucuronidase), 5′-GCGTGGAGCAAGACAGTGGGC-3′ and 5′-GCGTGGAGCAAGACAGTGGGC-3′. The relative amounts of *SDC4* mRNA were calculated using a standard curve generated using a plasmid containing the gene of interest. All samples were normalized to *GUSB* mRNA.

Plasmid construction

A HindIII/NcoI fragment (from −1563 to +1) of the human *SDC4* (with A of the ATG translation initiation codon as +1) was cloned into a luciferase reporter plasmid, pGL4.10 (Promega, Madison, WI, USA). A series of deletion constructs, termed pSDC4-544, pSDC4-370, pSDC4-217 and pSDC4-151, were generated by digestion with restriction enzymes. Mutated constructs (MT −191/−182, MT −137/−127, MT double) were prepared by the QuikChange Lightning Site-Directed Mutagenesis Kit (Stratagene, La Jolla, CA, USA) according to the manufacturer's instructions using the following primers: MT−191/−182, 5′-CGGGTCCCTTAAGGTTTCCAACTCCGCGGGC-3′ and 5′-CGCCCGCGGAGTTGGAAACCTTAAGGGACCC-3′ and MT −137/−127, 5′-GGCCTCGCTTCCACTGAAGAATTCCGGGCGGGGTG-3′ and 5′-CCCGCCCGGAATTCTTCAGTGGAAGCGAGGCCTGC-3′.

Transfection and luciferase reporter assays

EAhy926 cells (1.0×10^5 cells) were plated on 35-mm dishes and grown to sub-confluence (overnight). Co-transfection with 200 ng of luciferase reporter plasmids and 100 ng of pGL4.74 (hRluc/TK) vector (Promega), used as an internal control, was performed using Lipofectamine 2000 (Invitrogen). After 6 h, the transfection media was replaced with fresh DMEM supplemented with 10% FBS. The cells were incubated overnight and then treated with 10 ng/ml of recombinant human TNF-α for 3 h before harvesting. To measure luciferase activity of the transfected cells, Dual-Luciferase Reporter Assay System (Promega) was used according to the manufacturer's instructions. Firefly luciferase activity was normalized to the activity of co-transfected *Renilla* luciferase that was used as an internal control for transfection efficiency.

Immunofluorescence staining

EAhy926 cells were seeded on 18 × 18 mm cover glasses coated with collagen I (Nippi, Tokyo, Japan). After 24 h, cells were treated with TNF-α or fresh media for 30 min. Immunofluorescence staining was performed as described earlier (*16*). In brief, cells were fixed in cold methanol and then treated with cold acetone. Next, the cells were incubated with PBS containing 1% BSA for 30 min at room temperature and treated with rabbit anti-NF-κB p65 (C-20), anti-NF-κB p50 (H-119) or mouse anti-c-Rel (B-6) antibody (Santa Cruz Biotechnology) for 1 h at room temperature. After washing, the cells were treated with Alexa Fluor 488-conjugated goat anti-rabbit IgG (H+L) or AlexaFluor488-conjugated goat anti-mouse IgG (H+L) antibody (Invitrogen) for 60 min at room temperature. Then, the cells were mounted using VECTASHIELD with DAPI (Vector Laboratories Inc., Burlingame, CA, USA) and inspected by fluorescence microscopy (PROVISAX80, OLIMPUS, Tokyo, Japan).

Preparation of nuclear extracts

After TNF-α treatment, harvested cells were resuspended in lysis buffer [10 mM HEPES pH 7.9, 1.5 mM $MgCl_2$, 10 mM KCl, 1 mM DTT and protease inhibitor cocktail (Nakarai Tesque, Kyoto, Japan)], disrupted by passing through a syringe five times and centrifuged for 20 min. The supernatant, containing cytoplasm proteins, was stored at −80°C for later use. To extract nuclear proteins, the pellets were resuspended in extraction buffer (20 mM HEPES pH 7.9, 1.5 mM $MgCl_2$, 0.42 M NaCl, 0.2 mM EDTA, 25% glycerol, 1 mM DTT and protease inhibitor cocktail) for 30 min on ice. After centrifugation for 5 min, the supernatant was collected and stored at −80°C for later use.

Western blot analysis

Nuclear or cytoplasmic extracts were run on a 10% SDS–PAGE gel and transferred to immobilon-P membranes (Millipore, Bedford, MA, USA). Rabbit anti-NF-κB p65 (C-20), anti-NF-κB p50 (H-119), anti-lamin A/C antibody (Santa Cruz Biotechnology), mouse anti-c-Rel (B-6) antibody, anti-phospho-NF-κB p65 (Ser536) (7F1) antibody (Cell Signaling Technology, Danvers, MA, USA) or anti-α-tubulin antibody (Sigma-Aldrich) was used as a primary antibody, and horseradish peroxidase-conjugated antibodies (Cell Signaling Technology) were used as secondary antibodies. A chemiluminescent substrate (ECL Plus Western Blotting Detection System, Amersham Biosciences, Piscataway, NJ, USA) was used to identify the relevant bands.

Electrophoretic mobility shift assay

Nuclear extracts were prepared as described earlier. Oligonucleotides containing the *SDC4* promoter fragment (from −198 to −172 and from −149 to −123) were synthesized, biotinylated and annealed. Electrophoretic mobility shift assay (EMSA) was performed using a LightShift Chemiluminescent EMSA Kit (Pierce, Rockford, IL, USA) according to the manufacture's protocol. In brief, the nuclear extracts (2.4 μg) and biotin-labelled double-strand oligonucleotides (300 fmol) were incubated at room temperature for 1 h. Competition experiments were performed similarly with the addition of a 100-fold excess of unlabelled competitor oligonucleotides. In a supershift assay, the nuclear extract was incubated with anti-p65 antibody, anti-p50 antibody, anti-c-Rel antibody or normal rabbit IgG for 20 min after oligonucleotide incubation. The reaction mixture was subjected to electrophoresis on a 6% non-denaturing polyacrylamide gel, transferred to a Hybond-N+ membrane (GE Healthcare UK Ltd., England) and cross-linked to the membrane by UV light. Bands were detected using a chemiluminescent substrate as described earlier.